

1 **Optical diode effect at telecom wavelengths in a polar magnet**

2 Kevin A. Smith,¹ Yanhong Gu,¹ Xianghan Xu,² Heung-Sik Kim,³

3 Sang-Wook Cheong,^{2,4} Scott A. Crooker,⁵ and Janice L. Musfeldt^{1,6,*}

4 ¹*Department of Chemistry, University of Tennessee, Knoxville, Tennessee 37996, USA*

5 ²*Department of Physics and Astronomy,*

6 *Rutgers University, Piscataway, NJ 08854, USA*

7 ³*Department of Semiconductor Physics and Institute of Quantum Convergence Technology,*

8 *Kangwon National University, Chuncheon 24341, Republic of Korea*

9 ⁴*Keck Center for Quantum Magnetism,*

10 *Rutgers University, Piscataway, New Jersey 08854 USA*

11 ⁵*National High Magnetic Field Laboratory, Los Alamos, NM 87545, USA*

12 ⁶*Department of Physics and Astronomy,*

13 *University of Tennessee, Knoxville, TN 37996, USA*

14 **Abstract**

15 Magnetolectric multiferroics such as rare earth manganites host nonreciprocal be-
16 havior driven by low symmetry, spin-orbit coupling, and toroidal moments, although
17 less has been done to explore whether lanthanides like Er^{3+} might extend functionality
18 into the hard infrared for optical communications purposes. In this work, we reveal
19 nonreciprocity in the f -manifold crystal field excitations of $h\text{-Lu}_{0.9}\text{Er}_{0.1}\text{MnO}_3$. In addi-
20 tion to contrast in the highest fields, we demonstrate nonreciprocity at technologically-
21 relevant energy scales - specifically in the E-, S-, and C-bands of the telecom wave-
22 length range - and at low magnetic fields and room temperature. In fact, the low field
23 behavior is consistent with possible altermagnetism. These findings advance the over-
24 all understanding of localized excitations in rare earth-containing systems and pave
25 the way for entirely new types of telecom applications.

* musfeldt@tennessee.edu

26 **INTRODUCTION**

27 Nonreciprocal directional dichroism is a type of asymmetric light absorption that de-
28 pends upon propagation direction.^{1,2} It is a defining feature of materials that simulta-
29 neously break spatial inversion and time-reversal symmetries.^{3,4} Although discovered in
30 magnetoelectrics including CuB₂O₄,⁵⁻⁸ FeZnMo₃O₈,⁹ LiNiPO₄,¹⁰ LiCoPO₄,¹¹ Nd₂Ti₂O₇,¹²
31 Pb(TiO)Cu₄(PO₄)₄,¹³ and Ni₃TeO₆,¹⁴⁻¹⁶ nonreciprocity is under-explored in rare earth-
32 containing systems. This is because *f*-manifold crystal field excitations (which are both
33 spin- and parity-forbidden) have been presumed not to host large nonreciprocal effects even
34 though mixing of electric and magnetic dipoles at noncentrosymmetric rare earth sites can
35 generate significant magnetoelectric coupling.^{1,17} Properties arising from Er³⁺ are especially
36 relevant to amplifiers, isolators, modulators, and rectifiers at optical communications wave-
37 lengths.¹⁸⁻²⁷ The prospect of integrating additional functionality in the form of nonreciprocity
38 to the rare earth excitations that power these telecommunications technologies is therefore
39 both challenging and potentially transformative. Rather than testing drawn quartz fibers
40 sprinkled with powdered Er,^{22,23} we employed *h*-Lu_{0.9}Er_{0.1}MnO₃ as a platform for examining
41 whether rare earth *f*-manifold excitations have the potential to host nonreciprocal behavior
42 in the hard infrared. This system sports a dilute ensemble of Er³⁺ ions within a *P*6₃*mc* ma-
43 trix that combines spontaneous polarization along *c* (arising from improper ferroelectricity
44 involving the Mn centers) with antiferromagnetism due to Mn³⁺ ordering (*T*_N ≈ 80 K) and
45 a rare earth related transition near 30 K [Fig. 1a].^{28,29} In fact, *h*-Lu_{0.9}Er_{0.1}MnO₃ is likely
46 an altermagnet due to antisymmetric spin splitting in the 6'mm' magnetic ground state.³⁰
47 Our work is enabled by the development of monopolar domain single crystals which grow
48 in a characteristic canopy-like shape [Fig. 1b]. Such a material - if functioning as a secure
49 communications element - should host higher fidelity and lower loss than glass fibers with
50 Er randomly distributed throughout.

51 The symmetry requirements for toroidal nonreciprocity in *h*-Lu_{0.9}Er_{0.1}MnO₃ dictate that
52 polarization, magnetic field, and light propagation direction must be mutually orthogo-
53 nal.^{1,4,16} We therefore performed magneto-optical spectroscopy in this fashion. Strikingly,
54 these measurements reveal strong nonreciprocal behavior in the *f*-manifold crystal field ex-
55 citations of Er³⁺ that persists not only at high fields but also at modest magnetic fields and

56 even up to room temperature. At 1525 nm, we find a contrast of 3.2% at 1.2 T and 296 K.
57 These findings challenge the conventional wisdom about localized excitations, opening the
58 door to entirely new types of nonreciprocal behavior and applications.

59 RESULTS AND DISCUSSION

60 Er³⁺ crystal field excitations in the hard infrared

61 Figure 1c,d displays the near infrared absorption of *h*-Lu_{0.9}Er_{0.1}MnO₃ as a function of
62 temperature. This particular wavelength range focuses on the Er³⁺ *f*-manifold crystal field
63 excitations in the E-, S-, and C-bands of the telecom range. These excitations are well-known
64 to be sharp and highly localized. The clusters of peaks between 1440 and 1540 nm can be
65 assigned as $^4I_{15/2} \rightarrow ^4I_{13/2}$. This set of excitations is well-studied in Er-containing oxides,
66 chalcogenides, and silica glasses^{20-25,31} because the excitations are responsible for the sub-
67 stantial gain near 1550 nm in Er-doped fiber amplifiers for long-range optical communication.
68 *h*-Lu_{0.9}Er_{0.1}MnO₃ contains two unique Er³⁺ centers, each with seven primary $^4I_{15/2} \rightarrow ^4I_{13/2}$
69 excitations at base temperature, with additional features arising from temperature-induced
70 population effects. The two Er³⁺ sites and the combination of both *ab*-plane and *c*-oriented
71 excitations add to the complexity of the 4 K data. The impact of population effects along
72 with the Er³⁺-related and Mn³⁺ magnetic ordering transition is evident in the contour plot
73 as well.^{30,32}

74 Nonreciprocity in *f*-manifold crystal field excitations

75 In order to explore how low symmetry and spin-orbit coupling impact the properties
76 of *f*-manifold crystal field excitations, we measured the magneto-optical response of *h*-
77 Lu_{0.9}Er_{0.1}MnO₃ at base and room temperatures and calculated the nonreciprocity which
78 is defined as $\Delta\alpha_{\text{NDD}} = \alpha(+H, +k) - \alpha(-H, +k)$. Figure 2 summarizes these results in the
79 form of contour plots. As anticipated, the excitations shift linearly in magnetic field with
80 different slopes given by the respective *g* factors. We find features that cross and merge as
81 well as excitations that host avoided crossings. The latter defines critical fields at 6 and 30
82 T, in line with the magnetization of *h*-ErMnO₃^{30,32} as well as our own measurements of *h*-

83 $\text{Lu}_{0.9}\text{Er}_{0.1}\text{MnO}_3$ [Fig. S6, Supplementary Information]. The key point is that nonreciprocity
84 is observed at both low fields and high temperatures and is sensitive to the development of
85 different field-induced magnetic states.

86 Figure 3 summarizes the dichroic spectra of $h\text{-Lu}_{0.9}\text{Er}_{0.1}\text{MnO}_3$. These data were taken
87 in the toroidal configuration with $\pm H$ which is symmetrically equivalent to $\pm k$ [Fig. S2,
88 Supplementary Information].³³ As a reminder, toroidal dichroism occurs when light propa-
89 gation is along the toroidal moment T , ($\vec{k} \parallel T = P \times M$, where P and M are the electric
90 polarization and magnetic moment).^{3,34-38} We polished and mounted our crystal consistent
91 with this configuration [Fig. S1, Supplementary Information].

92 Figure 3a displays the nonreciprocal directional dichroism of $h\text{-Lu}_{0.9}\text{Er}_{0.1}\text{MnO}_3$ at 5.5 K,
93 well below the Er^{3+} -related transition and magnetic ordering temperature of Mn^{3+} . The
94 dichroic response is unexpectedly large (18.8% at 1516 nm and 55 T) for such a highly
95 localized set of excitations. These results unequivocally confirm that f -manifold crystal field
96 excitations in a magnetoelectric material can host nonreciprocity. The effect is sharp and
97 clear, with a very systematic response as a function of applied magnetic field. Even more
98 remarkably, we find that this system does not need the highest fields to reveal functionality.
99 $\Delta\alpha_{\text{NDD}}$ is approximately 10.4% at 1525 nm and 1.2 T. That such a well-defined nonreciprocal
100 effect can be observed in the telecom wavelength range allows us to conceive of a number of
101 unique opportunities.

102 To test the impact of magnetic ordering on the dichroic effect, we performed similar
103 experiments at elevated temperatures. Figure 3b,c displays the nonreciprocal directional
104 dichroism of $h\text{-Lu}_{0.9}\text{Er}_{0.1}\text{MnO}_3$ at 31 and 186 K, respectively. There is no rare earth ordering
105 at 31 K,^{30,32} although the Mn^{3+} centers are still magnetically ordered ($T_N \approx 80$ K). Even so,
106 nonreciprocity is surprisingly strong. Increasing temperature to 186 K eliminates magnetic
107 ordering involving the Mn^{3+} sites as well. The consequence is a substantial decrease in
108 the size of the dichroic signal. The overall shape changes due to population effects as well.
109 Clearly, $\text{Er}\cdots\text{Mn}$ interactions are important - but not essential - for this process.

110 **Nonreciprocity at room temperature**

111 Inspired by the possibility that a well-ordered magnetic state is not required for the devel-
112 opment of nonreciprocity in *f*-manifold crystal field excitations, we measured the magneto-
113 optical properties of *h*-Lu_{0.9}Er_{0.1}MnO₃ at room temperature. As a reminder, nonreciprocal
114 directional dichroism requires magnetoelectric coupling. This is because the magnetoelec-
115 tric susceptibility $\chi_{\alpha\beta}^{me}$ is proportional to $\langle 0|P_\alpha|n\rangle\langle n|M_\beta|0\rangle$, so both the polarization and
116 magnetization matrix elements must be non-zero.¹

117 Figure 3d displays the dichroic response of *h*-Lu_{0.9}Er_{0.1}MnO₃ at room temperature. Strik-
118 ingly, the effect is not quenched due to a lack of long-range magnetic order in the Mn frame-
119 work. This is because the toroidal configuration does not require magnetic order since $\vec{k} \parallel$
120 $T = P \times M$.^{3,34,36-39} Examination reveals that $\Delta\alpha_{NDD}$ is still as high as 13.7% at 1516 nm
121 and full field, although the exact magnitude varies depending upon the excitation, and the
122 overall size of the spectral features are much more field sensitive than before. Not only is the
123 signal larger in higher fields, but the highest fields are needed to obtain well-formed peak
124 shapes. This is likely because larger fields are required to overcome thermal fluctuations,
125 align Er moments, and break time-reversal symmetry in the paramagnetic phase above the
126 ordering temperature. Even at 296 K, *h*-Lu_{0.9}Er_{0.1}MnO₃ continues to host nonreciprocal di-
127 rectional dichroism at very modest fields. $\Delta\alpha_{NDD}$ at 1.2 T, for instance, is still distinct [inset,
128 Fig. 3d]. These findings demonstrate that it is indeed possible to realize room temperature
129 nonreciprocity under low field conditions in the telecom range.

130 **Breaking time reversal symmetry in this system**

131 Thus far, we have seen that at low temperatures, where Mn is antiferromagnetically
132 ordered, Er \cdots Mn interactions break time-reversal symmetry to enable nonreciprocity in the
133 *f*-manifold excitations. We speculate that, in the presence of magnetic order, the Mn-induced
134 local exchange fields on the Er moments cooperate with the external field for an enhanced
135 dichroic response. This provides a way to understand the dramatic spectral changes across
136 the Mn ordering temperature. Below the ordering temperature, *h*-Lu_{0.9}Er_{0.1}MnO₃ likely
137 exhibits *B*₂-type symmetry, corresponding to a 6'mm' magnetic point group, suggesting the
138 potential for symmetric and antisymmetric spin splitting (S/A-type altermagnetism).⁴⁰ This

139 may provide a possible explanation for the substantial enhancement of the nonreciprocal
140 signal below T_N [Fig. S4, Supplementary Information]. At higher temperatures, where Mn
141 is no longer ordered, the applied field acts on the Er moments directly to break time reversal
142 symmetry, the result generating a smaller, yet still appreciable nonreciprocal signature - even
143 at room temperature. These effects are well within the limits of our sensitivity. Due to the
144 low energy scales for *f*-orbital excitations, small external perturbations lead to a remarkably
145 large nonreciprocal response, 3.2% at 1525 nm and 1.2 T, even at room temperature.

146 To summarize, we report the discovery of nonreciprocity in the rare earth crystal field
147 excitations of an Er^{3+} -containing oxide across the telecom wavelength range. The effect is
148 surprisingly strong - a finding that we attribute to the ability of the applied field to rotate
149 Er^{3+} moments. At the same time, there is a polar environment around the noncentrosym-
150 metric rare earth ions leading to the formation of net toroidal moments even in the presence
151 of very small magnetic fields. While there is some sensitivity to magnetic ordering likely
152 due to altermagnetic character below T_N , the toroidal configuration generally supports low
153 loss nonreciprocity in monopolar crystals of $h\text{-Lu}_{0.9}\text{Er}_{0.1}\text{MnO}_3$ at readily accessible fields and
154 temperatures - including room temperature. These findings open the door to the develop-
155 ment of structure-property relations as well as low power devices in this unique application
156 space.

157 METHODS

158 **Single crystal growth:** $h\text{-Lu}_{0.9}\text{Er}_{0.1}\text{MnO}_3$ powder was synthesized by sintering a stoichio-
159 metric mixture of Lu_2O_3 , Er_2O_3 , and Mn_2O_3 powders at 1350 °C for 30 hours, with two
160 intermediate grindings. For single crystal growth, the synthesized powder was mixed with
161 Bi_2O_3 flux in a molar ratio of 1:10. The mixture was placed in a platinum crucible, heated
162 to 1100 °C for 10 hours, then cooled at a rate of 2 °C per hour to 800 °C, followed by rapid
163 cooling at 100 °C per hour to room temperature. The residual flux was removed using dilute
164 hydrochloric acid to isolate $h\text{-Lu}_{0.9}\text{Er}_{0.1}\text{MnO}_3$ crystals. Compared to previously reported flux
165 growth methods that yielded multi-ferroelectric-domain crystals, the approach used here in-
166 corporates a higher ratio of Bi_2O_3 flux. As a result, crystallization occurred at the surface
167 rather than at the bottom of the crucible. This surface crystallization effectively poled the

168 crystals into a single ferroelectric domain, as confirmed by optical microscope images of the
169 chemically etched surfaces. The crystals were polished to reveal the *c*-axis (since the polar
170 *c*-axis is normal to the large natural growth face) and to obtain a proper optical density for
171 our experiments. In this case, the thickness was 230 μm . This configuration is shown in Fig.
172 S1, Supplementary Information.

173 **Spectroscopic techniques:** Spectroscopic measurements at zero magnetic field were per-
174 formed using a Bruker Equinox 55 Fourier-transform infrared spectrometer across the in-
175 frared range from 800 - 2600 nm, more than covering the telecom wavelengths (1260 -
176 1625 nm) and the response of the *f*-manifold excitations in that vicinity. Unpolarized
177 light was used for all experiments. The absorption coefficient was calculated as: $\alpha(\lambda) =$
178 $(-1/d)\ln(\mathcal{T}(\lambda))$, where \mathcal{T} is the measured normalized transmission, and d is the crystal
179 thickness. An open-flow cryostat was used for temperature control.

180 **Magneto-optical measurements:** Magneto-optical spectroscopy was performed at cryo-
181 genic temperatures using a 65 T pulsed magnet at the National High Magnetic Field Labora-
182 tory in Los Alamos, NM. The samples were mounted in the Voigt geometry on a fiber-coupled
183 probe. Two multi-mode optical fibers were used to deliver broadband, unpolarized, white
184 light to the sample, and to collect the light transmitted through the sample, respectively.
185 The collected light was dispersed in a 300 mm spectrometer, using a 600 groove/mm grat-
186 ing, and was detected by a 1024-pixel InGaAs array detector. We focused on the E-, S-,
187 and C-bands of the telecom wavelength range (1460 - 1565 nm), achieving approximately
188 0.1 nm spectral resolution to capture changes in the sharp *f*-manifold excitations. To test
189 nonreciprocal directional dichroism, the propagation direction of the light ($\pm k$) through the
190 sample was reversed by switching the delivery and collection fibers and also by reversing
191 the direction of the magnetic field ($\pm H$). A comparison is shown in Fig. S2, Supplemen-
192 tary Information. We provide an example of the raw data collected at ± 55 T in Fig. S3,
193 Supplementary Information.

194 **DATA AVAILABILITY**

195 The datasets generated and/or analyzed during the current study are not publicly available
196 due to active intellectual property considerations, but are available from the corresponding

197 authors upon reasonable request.

198 **ACKNOWLEDGMENTS**

199 Research at the University of Tennessee is supported by Condensed Matter Physics, Di-
200 vision of Materials Research, U. S. National Science Foundation (DMR-2226109). Work
201 at Rutgers is funded by the W. M. Keck foundation grant to the Keck Center for Quan-
202 tum Magnetism at Rutgers University. The National High Magnetic Field Laboratory is
203 supported by the National Science Foundation Cooperative Agreement DMR-2128556, the
204 State of Florida, and the U.S. Department of Energy. HSK was supported by the Basic
205 Science Research Program through the National Research Foundation of Korea funded by
206 the Ministry of Science and ICT [Grant No. NRF-2020R1C1C1005900, RS-2023-00220471].

207 **AUTHOR CONTRIBUTIONS**

208 JLM and SWC designed the study. XX grew the crystals under the supervision of SWC.
209 KAS, SAC, and JLM performed the pulsed field magneto-optical spectroscopies. KS and
210 YG analyzed the data with guidance from JLM. KAS and JLM developed the figures and
211 wrote the manuscript. KAS, YG, XX, HSK, SWC, SAC, and JLM commented on the text.

212 **COMPETING INTERESTS**

213 Authors KAS, YG, XX., HSK, SAC, and JLM declare no competing interests. SWC serves
214 as an editor of this journal and had no role in the peer-review or decision to publish this
215 paper. SWC declares no competing interests.

216 **REFERENCES**

217 [1] Kézsmárki, I. *et al.* One-way transparency of four-coloured spin-wave excitations in multiferroic
218 materials. *Nat. Commun.* **5**, 3203 (2014). URL <https://doi.org/10.1038/ncomms4203>.

219 [2] Tokura, Y. & Nagaosa, N. Nonreciprocal responses from non-centrosymmetric quantum mate-
220 rials. *Nat. Commun.* **9**, 3740 (2018). URL <https://doi.org/10.1038/s41467-018-05759-4>.

221 [3] Narita, H. *et al.* Observation of nonreciprocal directional dichroism via electromagnon reso-
222 nance in a chiral-lattice helimagnet $\text{Ba}_4\text{NbFe}_3\text{Si}_2\text{O}_{14}$. *Phys. Rev. B* **94**, 094433 (2016). URL
223 <https://link.aps.org/doi/10.1103/PhysRevB.94.094433>.

224 [4] Cheong, S.-W. & Huang, F.-T. Trompe L’oeil ferromagnetism—magnetic point group analysis.
225 *npj Quantum Mater.* **8**, 73 (2023). URL <https://doi.org/10.1038/s41535-023-00603-5>.

226 [5] Saito, M., Ishikawa, K., Taniguchi, K. & Arima, T. Magnetic control of crystal chirality and
227 the existence of a large magneto-optical dichroism effect in CuB_2O_4 . *Phys. Rev. Lett.* **101**,
228 117402 (2008). URL <https://link.aps.org/doi/10.1103/PhysRevLett.101.117402>.

229 [6] Toyoda, S., Abe, N. & Arima, T. Gigantic directional asymmetry of luminescence in multifer-
230 roic CuB_2O_4 . *Phys. Rev. B* **93**, 201109 (2016). URL <https://link.aps.org/doi/10.1103/PhysRevB.93.201109>.

232 [7] Nikitchenko, A. I. & Pisarev, R. V. Magnetic and antiferromagnetic nonreciprocity of light
233 propagation in magnetoelectric CuB_2O_4 . *Phys. Rev. B* **104**, 184108 (2021). URL <https://link.aps.org/doi/10.1103/PhysRevB.104.184108>.

235 [8] Boldyrev, K. N. *et al.* Nonreciprocity of optical absorption in the magnetoelectric antiferromag-
236 net CuB_2O_4 . *Magnetochemistry* **9** (2023). URL <https://www.mdpi.com/2312-7481/9/4/95>.

237 [9] Yu, S. *et al.* High-temperature terahertz optical diode effect without magnetic order in polar
238 $\text{FeZnMo}_3\text{O}_8$. *Phys. Rev. Lett.* **120**, 037601 (2018). URL <https://link.aps.org/doi/10.1103/PhysRevLett.120.037601>.

240 [10] Kimura, K. & Kimura, T. Nonvolatile switching of large nonreciprocal optical absorption at
241 shortwave infrared wavelengths. *Phys. Rev. Lett.* **132**, 036901 (2024). URL <https://link.aps.org/doi/10.1103/PhysRevLett.132.036901>.

243 [11] Tóth, B. *et al.* Imaging antiferromagnetic domains in LiCoPO_4 via the optical magnetoelec-
244 tric effect. *Phys. Rev. B* **110**, L100405 (2024). URL <https://link.aps.org/doi/10.1103/PhysRevB.110.L100405>.

246 [12] Shimada, Y., Kiyama, H. & Tokura, Y. Nonreciprocal directional dichroism in ferroelectric
247 $\text{Nd}_2\text{Ti}_2\text{O}_7$. *J. Phys. Soc. Jpn.* **77**, 33706 (2008). URL <https://doi.org/10.1143/JPSJ.77.033706>.

[13] Katsuyoshi, T. *et al.* Nonreciprocal directional dichroism in a magnetic-field-induced ferroelectric phase of $\text{Pb}(\text{TiO})\text{Cu}_4(\text{PO}_4)_4$. *J. Phys. Soc. Jpn.* **90**, 123701 (2021). URL <https://doi.org/10.7566/JPSJ.90.123701>.

[14] Yokosuk, M. O. *et al.* Nonreciprocal directional dichroism of a chiral magnet in the visible range. *npj Quantum Mater.* **5**, 20 (2020). URL <https://doi.org/10.1038/s41535-020-0224-6>.

[15] Sirenko, A. A. *et al.* Total angular momentum dichroism of the terahertz vortex beams at the antiferromagnetic resonances. *Phys. Rev. Lett.* **126**, 157401 (2021). URL <https://link.aps.org/doi/10.1103/PhysRevLett.126.157401>.

[16] Park, K. *et al.* Nonreciprocal directional dichroism at telecom wavelengths. *npj Quantum Mater.* **7**, 38 (2022). URL <https://doi.org/10.1038/s41535-022-00438-6>.

[17] Gao, Y. & Xiao, D. Nonreciprocal directional dichroism induced by the quantum metric dipole. *Phys. Rev. Lett.* **122**, 227402 (2019). URL <https://link.aps.org/doi/10.1103/PhysRevLett.122.227402>.

[18] Tanabe, S. Rare-earth-doped glasses for fiber amplifiers in broadband telecommunication. *C. R. Chim.* **5**, 815–824 (2002). URL <https://www.sciencedirect.com/science/article/pii/S1631074802014492>.

[19] Ulanowski, A., Merkel, B. & Reiserer, A. Spectral multiplexing of telecom emitters with stable transition frequency. *Sci. Adv.* **8**, eabo4538 (2022). URL <https://www.science.org/doi/abs/10.1126/sciadv.abo4538>.

[20] Della Valle, F. & Modesti, S. Exchange-excited $f - f$ transitions in the electron-energy-loss spectra of rare-earth metals. *Phys. Rev. B* **40**, 933–941 (1989). URL <https://link.aps.org/doi/10.1103/PhysRevB.40.933>.

[21] Florez, A., Messaddeq, Y., Malta, O. & Aegerter, M. Optical transition probabilities and compositional dependence of Judd-Ofelt parameters of Er^{3+} ions in fluoroindate glass. *J. Alloys Compd.* **227**, 135–140 (1995). URL <https://www.sciencedirect.com/science/article/pii/0925838895016139>.

[22] Desurvire, E. *Erbium-doped fiber amplifiers: principles and applications* (John Wiley & Sons, Inc., New York, NY, 1994).

278 [23] Wang, Q., Dutta, N. K. & Ahrens, R. Spectroscopic properties of Er doped silica glasses. *J.*
279 *Appl. Phys.* **95**, 4025–4028 (2004). URL <https://doi.org/10.1063/1.1669056>.

280 [24] Rao, R. *et al.* Multi-band luminescence from a rare earth-based two-dimensional material.
281 *Matter* **8**, 101929 (2025). URL <https://www.sciencedirect.com/science/article/pii/S2590238524005988>.

283 [25] Zhai, Z. & Sahu, J. K. Progress in Er-doped fibers for extended L-band operation of amplifiers.
284 *Opt. Commun.* **578**, 131510 (2025). URL <https://www.sciencedirect.com/science/article/pii/S0030401825000380>.

286 [26] Xin, F. *et al.* Observation of extreme nonreciprocal wave amplification from single soliton-
287 soliton collisions. *Phys. Rev. A* **100**, 043816 (2019). URL <https://link.aps.org/doi/10.1103/PhysRevA.100.043816>.

289 [27] Puel, T. O., Turflinger, A. T., Horvath, S. P., Thompson, J. D. & Flatté, M. E. Enhancement
290 of microwave to optical spin-based quantum transduction via a magnon mode (2024). URL
291 <https://arxiv.org/abs/2411.12870>. 2411.12870.

292 [28] Palstra, T. T. M. *The magneto-electric properties of RMnO₃ compounds*, 391–399 (Springer
293 Berlin Heidelberg, Berlin, Heidelberg, 2007). URL https://doi.org/10.1007/11499893_23.

294 [29] Xu, L. *et al.* Strategy for achieving multiferroic E-type magnetic order in orthorhombic
295 manganites RMnO₃ (*R* = La–Lu). *Phys. Chem. Chem. Phys.* **22**, 4905–4915 (2020). URL
296 <http://dx.doi.org/10.1039/C9CP06275K>.

297 [30] Song, J. D. *et al.* Magnetization, specific heat, and thermal conductivity of hexagonal ErMnO₃
298 single crystals. *Phys. Rev. B* **96**, 174425 (2017). URL <https://link.aps.org/doi/10.1103/PhysRevB.96.174425>.

300 [31] Popova, M. N. *et al.* High-resolution optical spectroscopy and modeling of spectral and
301 magnetic properties of multiferroic ErFe₃(BO₃)₄. *Phys. Rev. B* **101**, 205108 (2020). URL
302 <https://link.aps.org/doi/10.1103/PhysRevB.101.205108>.

303 [32] Yen, F. *et al.* Magnetic phase diagrams of multiferroic hexagonal RMnO₃ (*R* = Er, Yb, Tm,
304 and Ho). *J. Mater. Res.* **22**, 2163–2173 (2007). URL <https://doi.org/10.1557/jmr.2007.0271>.

306 [33] Hlinka, J. Eight types of symmetrically distinct vectorlike physical quantities. *Phys. Rev. Lett.*
307 **113**, 165502 (2014). URL <https://link.aps.org/doi/10.1103/PhysRevLett.113.165502>.

308 [34] Rikken, G. L. J. A., Strohm, C. & Wyder, P. Observation of magnetoelectric directional
309 anisotropy. *Phys. Rev. Lett.* **89**, 133005 (2002). URL <https://link.aps.org/doi/10.1103/PhysRevLett.89.133005>.

310

311 [35] Cheong, S.-W., Talbayev, D., Kiryukhin, V. & Saxena, A. Broken symmetries, non-reciprocity,
312 and multiferroicity. *npj Quantum Mater.* **3**, 19 (2018). URL <https://doi.org/10.1038/s41535-018-0092-5>.

313

314 [36] Bordács, S. *et al.* Unidirectional terahertz light absorption in the pyroelectric ferrimagnet
315 CaBaCo₄O₇. *Phys. Rev. B* **92**, 214441 (2015). URL <https://link.aps.org/doi/10.1103/PhysRevB.92.214441>.

316

317 [37] Fishman, R. S. *et al.* Spin-induced polarizations and nonreciprocal directional dichroism of
318 the room-temperature multiferroic BiFeO₃. *Phys. Rev. B* **92**, 094422 (2015). URL <https://link.aps.org/doi/10.1103/PhysRevB.92.094422>.

319

320 [38] Ding, Q. *et al.* Parity-time symmetry in parameter space of polarization. *APL Photonics* **6**,
321 76102 (2021). URL <https://doi.org/10.1063/5.0051064>.

322

323 [39] Kézsmárki, I. *et al.* Enhanced directional dichroism of terahertz light in resonance with mag-
324 netic excitations of the multiferroic Ba₂CoGeO₇ oxide compound. *Phys. Rev. Lett.* **106**, 057403
325 (2011). URL <https://link.aps.org/doi/10.1103/PhysRevLett.106.057403>.

326

327 [40] Cheong, S.-W. & Huang, F.-T. Altermagnetism classification. *npj Quantum Mater.* **10**, 38
328 (2025). URL <https://doi.org/10.1038/s41535-025-00756-5>.

329

330 [41] Van Aken, B. B., Meetsma, A. & Palstra, T. T. M. Hexagonal LuMnO₃ revisited. *Acta
331 Crystallogr. E* **57**, i101–i103 (2001). URL <https://doi.org/10.1107/S1600536801015896>.

332

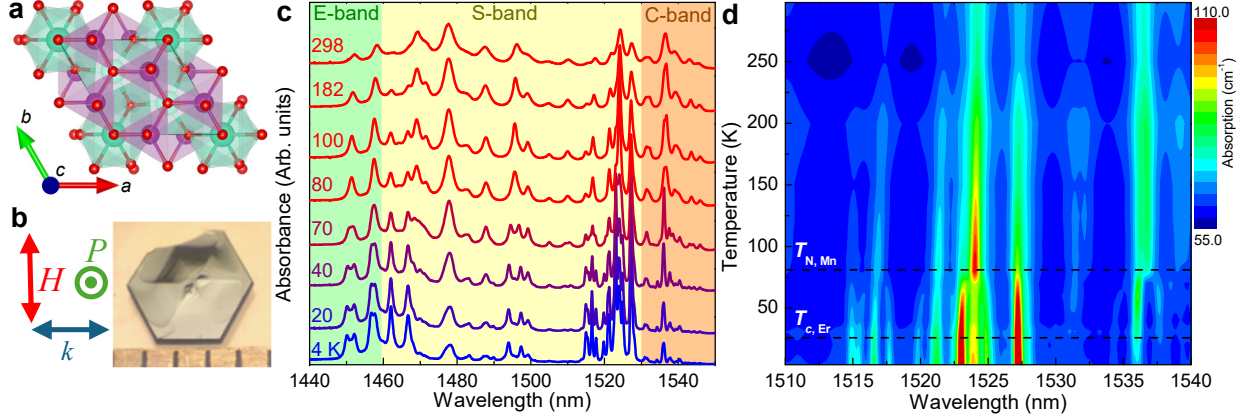


FIG. 1. Structure, measurement conditions, and temperature effects in *h*- $\text{Lu}_{0.9}\text{Er}_{0.1}\text{MnO}_3$. **a**, Crystal structure of *h*- $\text{Lu}_{0.9}\text{Er}_{0.1}\text{MnO}_3$ in the $P6_3mc$ space group.⁴¹ The Lu/Er, Mn, and O sites are indicated by teal, magenta, and red spheres, respectively. **b**, Schematic of the measurement geometry indicating the light propagation k , applied field H , and polarization P directions (left) and optical microscope image (right) of the ab -plane of the single crystal revealing the natural canopy-like structure that is indicative of a monopolar domain sample. Our single crystals were polished to expose the c -axis (which is the direction of polarization) as well as the $\perp c$ direction. Additional information about the orientation [Fig. S1], monopolar domain character [Fig. S5], and magnetic properties [Fig. S6] is provided in the Supplementary Information. **c**, Absorption of the $^4I_{15/2} \rightarrow ^4I_{13/2}$ rare earth crystal field excitations in *h*- $\text{Lu}_{0.9}\text{Er}_{0.1}\text{MnO}_3$ as a function of temperature with the corresponding telecom wavelength ranges indicated in green (E-band), yellow (S-band), and orange (C-band). The spectra are offset for clarity. **d**, Contour plot of the spectra in panel **c** with focus on the C-band features. The horizontal lines indicate Mn^{3+} antiferromagnetic ordering and the Er^{3+} -related transition.

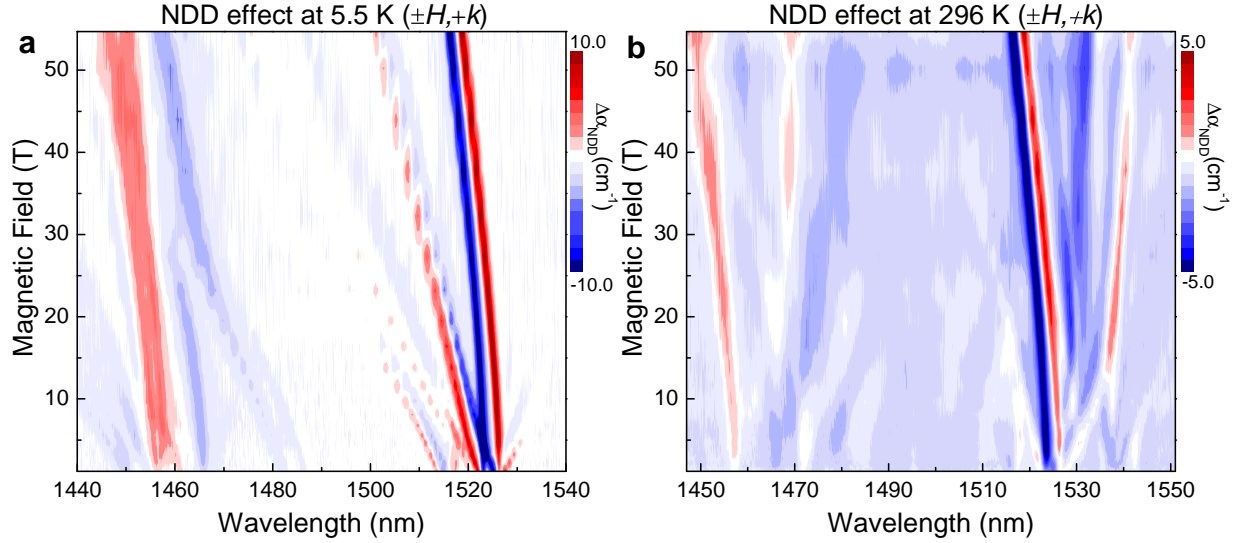


FIG. 2. **Color contour plots of dichroic effects.** Nonreciprocal directional dichroism of h - $\text{Lu}_{0.9}\text{Er}_{0.1}\text{MnO}_3$ at **a**, 5.5 K and **b**, room temperature (296 K) in a toroidal geometry in pulsed magnetic fields to 55 T and shown as contour plots. The color indicates the strength and sign of the dichroic signal. Nonreciprocal directional dichroism $\Delta\alpha_{\text{NDD}}$ is calculated as $\Delta\alpha_{\text{NDD}} = \alpha(+H, +k) - \alpha(-H, +k)$. This quantity is the difference between field pairs.

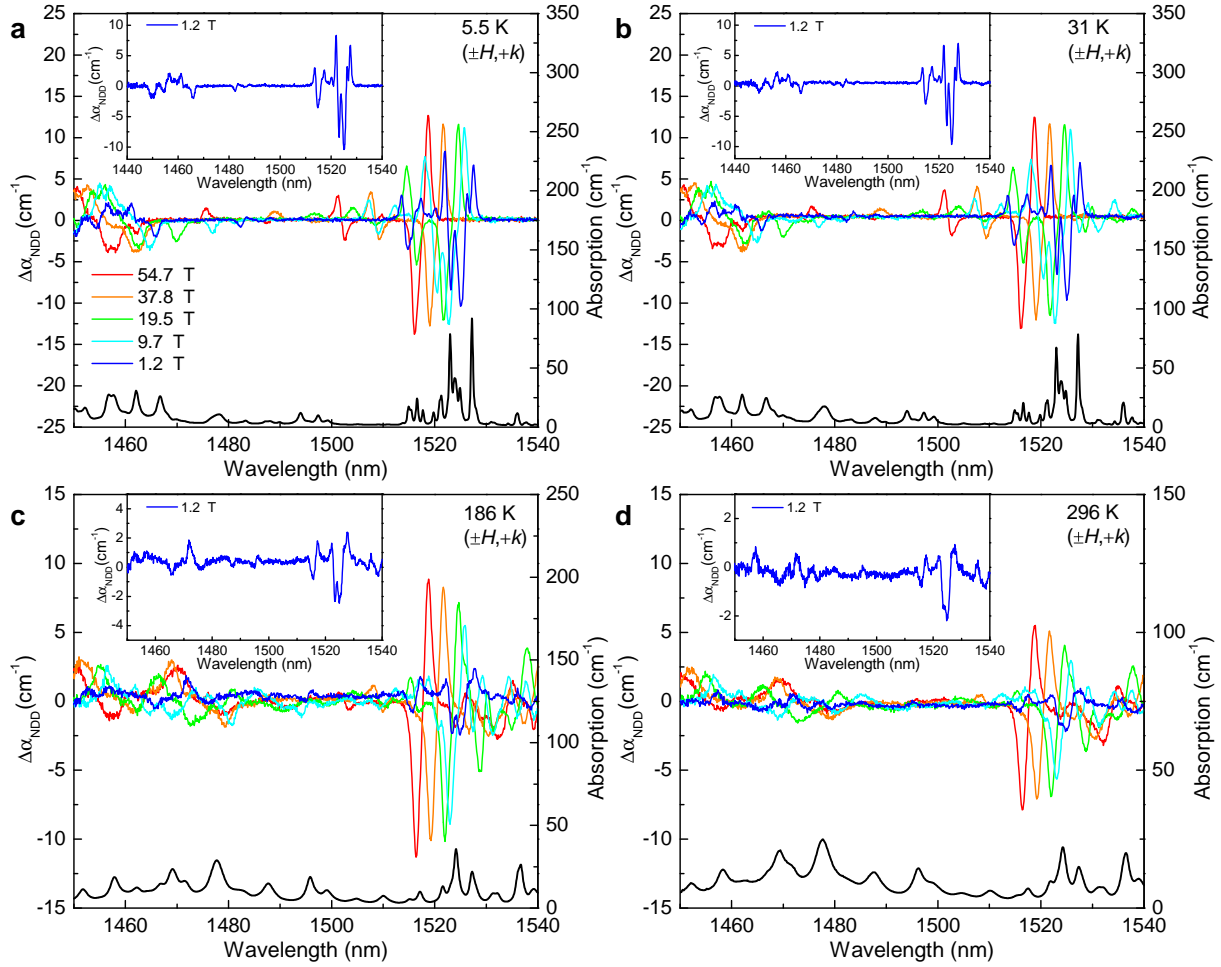


FIG. 3. **Temperature dependence of nonreciprocal directional dichroism.** Nonreciprocal directional dichroism of $h\text{-Lu}_{0.9}\text{Er}_{0.1}\text{MnO}_3$ at **a**, 5.5 K, **b**, 31 K, **c**, 186 K, and **d**, 296 K at selected fields. The absolute absorption at each temperature is at the bottom of each panel for comparison. These features are assigned as $\text{Er}^{3+} \ ^4I_{15/2} \rightarrow \ ^4I_{13/2}$ crystal field excitations. The insets show $\Delta\alpha_{\text{NDD}}$ at 1.2 T.